Adhesive dynamics of lubricated films

Fong Yew Leong* and K.-H. Chiam
*A*STAR Institute of High Performance Computing, 1 Fusionopolis Way, No. 16-16 Connexis, Singapore 138632, Singapore*
(Received 6 September 2009; revised manuscript received 29 March 2010; published 29 April 2010)

Membrane waves have been observed near the leading edge of a motile cell. Such phenomenon is the result of the interplay between hydrodynamics and adhesive dynamics. Here we consider membrane dynamics on a thin fluid gap supported by adhesive bonds. Using coupled lubrication theory and adhesive dynamics, we derive an evolution equation to account for membrane tension, bending, adhesion, and viscous lubrication. Four adhesion scenarios are examined: no adhesion, uniform adhesion, clustered adhesion, and focal adhesion. Two contrasting traveling wave types are found, namely, tension and adhesion waves. Tension waves disperse with time and space, whereas adhesion waves show increased amplitudes and are highly persistent. We show that the transition from tension to adhesion waves depends on a necessary, but insufficient, criterion that the wave amplitude must exceed a critical gap height, which is dependent on adhesion binding probability. We also show that strong adhesion results in sharp tension-to-adhesion wave transitions. The present work could explain the strong persistence of the waves observed in adhered cells using differential inference contrast (DIC) microscopy and the observation that the wavelengths decrease shortly after leading edge retraction.

DOI: 10.1103/PhysRevE.81.041923 PACS number(s): 87.17.Aa, 47.85.mf, 47.15.gm

I. INTRODUCTION

The phenomenon of membrane waves has been observed near the leading edge of a motile cell as a result of cyclical protrusion, adhesion, and retraction [1]. Periodic retraction offers an important means of testing the anchorage of the lamellipodium to the substrate for failure of adhesion at the tip leads to ruffling. Adhesion success at the tip, on the other hand, leads to cell edge retraction, as myosin II contracts, pulling the lamellipodial actin rearward [2]. This creates compressive stresses on the membrane layer behind the adhesion zone, leading to a fluid bulge traveling rearwards in a wavelike manner [3]. Such membrane waves are often the result of the interplay between hydrodynamics and adhesive dynamics.

A common description of the cell membrane is the Helfrich model [4,5], which has been successfully applied to studies on erythrocyte flickering [6] and extended to include hydrodynamic damping [7], confined membranes [8], anharmonic perturbations [9], and cytoskeletal [10] and wall interactions [11]. Other applications of the model include membrane fluctuations induced by membrane proteins of specific curvatures [12,13] and extended to account for membrane instabilities [14], actin polymerization [15] and myosin contraction [16]. These studies are successful in explaining the hydrodynamic fluctuations of the cell membrane [17], but they do not account for adhesive dynamics and lubrication effects.

Owing to the thin gap between the membrane and substrate, the hydrodynamics of the fluid film can be adequately described by the classical lubrication theory [18]. For the case of cell spreading or peeling on an adhesive surface, Hodges and Jensen [19] showed that the adhered front advances or retreats in a traveling wavelike manner. The same model was subsequently extended to account for effects of bond tilting [20]. Using Bell's kinetic theory [21] and Dembo's adhesive model [22], the adhesive forces can be described as a contact potential that is long-range attractive but short-range repulsive. This is similar to the conjoining or disjoining pressures one finds in extremely thin liquid films, where van der Waals forces are significant [23,24]. For a finite elastic sheet lubricated by such an extremely thin fluid film (e.g., MEMS), Hosoi and Mahadevan [25] have also shown that a peeling wave travels to the trailing edge, where pressure is vented and healing occurs rapidly.

Continuum adhesive dynamics models typically assume that binding molecules are uniformly distributed on surfaces [26–28]. However, it is known that adhesive structures tend to be clustered in the form of focal contacts or adhesions [29]. These adhesive structures are typically scattered along the cell periphery [30], which account for 5–15 % of the adhesion area [31]. The difference in mechanical strength was recognized by Ward and Hammer [32] who proposed a model of focal contact as an adhesive patch which fractures instead of peels under strong load. More recently, adhesive structures are broadly classified as uniformly distributed, clustered, and focal adhesion-associated bonds [33,34].

In the present paper, we model the cell membrane as a two-dimensional fluid-lubricated semi-infinite sheet. Through an imposed perturbation at the leading edge, we analyze traveling wave behavior governed by lubrication and adhesion effects. In addition, we account for nonuniformity in adhesive binding due to clustering and focal adhesions.

II. THEORY

A. Lubrication theory

The lubrication approximation for steady thin fluid film flows is written as

$$\partial_x p = \mu \partial_{zz} u, \tag{1}$$

where $p(x)$ is the fluid pressure, μ is the dynamic viscosity, $u(x,z)$ is the velocity in the x direction, and $h(x)$ is the gap

*leongfy@ihpc.a-star.edu.sg

height. The reference frame is set at the leading edge of the cell, which is advancing at a velocity of U due to actin protrusion so that

$$u(x,z) = \frac{h^2 \partial_x p}{2\mu}\left[\left(\frac{z}{h}\right)^2 - \left(\frac{z}{h}\right)\right] + U. \tag{2}$$

Since the flow rate $q=\int_0^h u dz$, and mass conservation requires $\partial_t h + \partial_x q = 0$, we can write the Reynolds lubrication equation [18] as

$$\partial_t h + U\partial_x h - \frac{1}{12\mu}\partial_x(h^3 \partial_x p) = 0. \tag{3}$$

B. Adhesive dynamics

Using Bell's kinetic theory [21], adhesion is modeled as a reversible chemical reaction $A_f \Leftrightarrow A_b$, where A_f is the density of free receptors and A_b is the density of bound receptors. The forward and reverse reaction rates are assumed to follow Boltzmann distribution [22]. If the reaction kinetics is rapid compared to the hydrodynamics, the density of bound receptors only depends on the gap height [19]. However, in the present paper, we also consider the effects of bond clustering, where bond density is greatest near the cell periphery [30]. The receptor site occupancy model [33] proposes a sigmoid-type bond distribution with distance, whereby bond density is saturated near the cell periphery and decreases significantly beyond the saturation distance. Thus, the local density of bound receptors is modeled as

$$A_b = A_t K_{eq} \phi(x) \exp\left[-\frac{\kappa}{2k_b T}(h-\lambda)^2\right], \tag{4}$$

where $A_t \equiv A_f + A_b$, K_{eq} is the chemical equilibrium constant, κ is the bond spring constant, λ is the equilibrium bond length, and $\phi(x) = [1+\exp[\eta(x-\chi)]]^{-1}$ is a bond distribution function, where η is the exponential prefactor of the sigmoid function and χ is the distance where the bond density is half of saturation value. For the case of uniform bond density, $\phi(x) \to 1$ and the equilibrium kinetics model [19] is recovered.

Each receptor bond modeled as a Hookean spring [22] so that the stress due to adhesion is

$$m = A_b \kappa (h - \lambda). \tag{5}$$

The pressure within the fluid layer is the sum of the contributions due to cell interior pressure, adhesion stress, membrane tension, and membrane bending rigidity [19],

$$p = p_c + m - \sigma \partial_{xx} h + \gamma \partial_{xxxx} h, \tag{6}$$

where p_c is the cell interior pressure, σ is the membrane tension, and γ is the membrane bending modulus.

C. Nondimensionalization

The following dimensionless variables and constants are now introduced,

$$X \equiv \frac{x}{L}, \quad H \equiv \frac{h}{\lambda}, \quad P \equiv \left(\frac{\lambda^2}{\mu U L}\right)p, \quad P_c \equiv \left(\frac{\lambda^2}{\mu U L}\right)p_c, \tag{7a}$$

$$\alpha \equiv \left(\frac{A_t K_{eq} \kappa \lambda^3}{\mu U L}\right), \quad \beta \equiv \left(\frac{\kappa \lambda^2}{k_b T}\right), \quad \bar{\sigma} \equiv \left(\frac{\lambda^3}{\mu U L^3}\right)\sigma, \tag{7b}$$

$$\bar{\gamma} \equiv \left(\frac{\lambda^3}{\mu U L^5}\right)\gamma,$$

$$\bar{\chi} \equiv \left(\frac{1}{L}\right)\chi, \quad \bar{\eta} \equiv L\eta, \tag{7c}$$

where $L \equiv U\tau$ is the length scale in the x direction and τ is the period of the wave.

Assuming $L \gg \lambda$, we express Eqs. (3) and (6) as a pair of evolution equations:

$$f(X,T) \equiv \partial_T H + \partial_X H - \frac{1}{12}\partial_X(H^3 \partial_X P) = 0, \tag{8a}$$

$$g(X,T) \equiv (P - P_c) - \alpha\phi\Delta H \exp\left(-\frac{\beta}{2}\Delta H^2\right) + \bar{\sigma}\partial_{XX} H - \bar{\gamma}\partial_{XXXX} H = 0, \tag{8b}$$

where $\Delta H \equiv H - 1$ is the deviation of the gap height from the equilibrium.

The exact physics governing the protrusion event is not well understood at this point [16]. Following a previously proposed Gaussian dip model for lateral membrane waves [16], we assume that the protrusion event can be described by a similar fixed point perturbation of the membrane at the leading edge. Therefore, the six boundary conditions required for the solution of the evolution equation are

$$H(0,T) = \begin{cases} 1 + \epsilon[1 - \cos(2\pi T)]/2, & T < 1 \\ 0, & T \geq 1 \end{cases}, \quad H(\infty,T) \to 1, \tag{9a}$$

$$\partial_{XX} H(0,T) = 0, \quad \partial_X H(\infty,T) \to 0, \tag{9b}$$

$$P(0,T) = P_0, \quad \partial_X P(\infty,T) \to 0, \tag{9c}$$

where ϵ is the peak-to-peak amplitude of the perturbation, α is a measure of adhesion strength, and β is a parameter governing adhesion probability.

The boundary conditions at the leading edge [Eq. (9), left] correspond to the fixed point perturbation produced by the protrusion event, no bending moment (pin connection) and a matched extracellular pressure. The boundary conditions far from the leading edge [Eq. (9), right] correspond to the equilibrium gap height, no height and no pressure gradient.

The evolution equation [Eq. (8)] is solved numerically on a finite difference scheme using implicit time stepping. The functions f and g are discretized in space via second-order central differencing and linearized around H and P in a $2n \times 2n$ Jacobian matrix, where n is the number of discretized nodes in the X direction. Iteration proceeds via Newton's method at each time step, until the relative error norms of H and P vectors reach a convergence threshold of 10^{-12}. For numerical accuracy, spatial resolution n is doubled and time

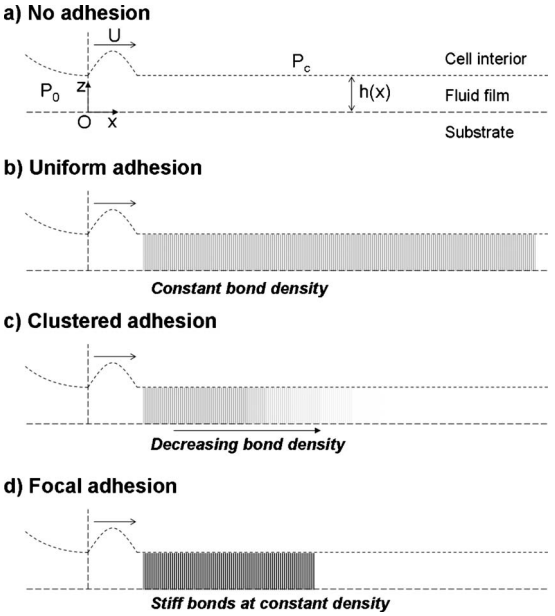

FIG. 1. Schematic of model geometry and adhesion scenarios.

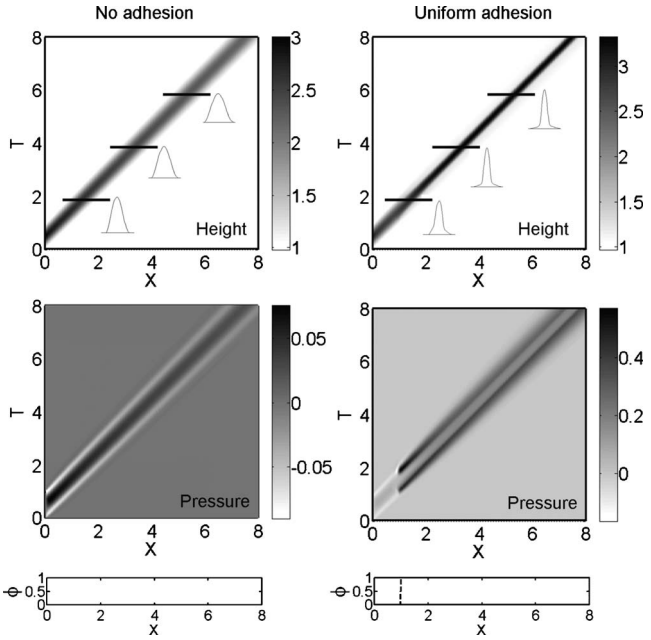

FIG. 2. Space-time plots of membrane height and pressure profile using perturbed amplitude $\epsilon=2$ and tension $\bar{\sigma}=1$. Bottom plots denote adhesive bond distribution $\phi(X)$. (Left) No adhesion ($\alpha=0$) promotes dispersive tension wave; (right) uniform adhesion ($\alpha=2$, $\beta=4$, $X\geq 1$) promotes stable adhesion wave. Insets show wave profiles at specific times indicated by the adjacent cuts.

step ΔT is halved until the relative error norms are less than 10^{-3}. The computational domain is restricted to $0\leq X\leq 10$, where $n=500$ and $\Delta T=0.1$.

III. RESULTS AND DISCUSSION

Consider a fixed point perturbation with a peak-to-peak amplitude of $\epsilon=2$ at the leading edge of the cell. Since pressure is scaled by a constant, we reference pressure at zero ($P_0=P_c=0$). Comparing typical values of membrane tension ($\sigma\sim 10^{-3}$ dyn/cm) and bending modulus ($\gamma\sim 10^{-12}$ dyn cm) [35,36], we set the tension coefficient as unity ($\bar{\sigma}=1$) for reference and the bending coefficient as a small parameter ($\bar{\gamma}=0.01$). However, note that the bending term is of significance at small length-scales (see Appendix A).

A. Adhesion scenarios

Distribution of adhesive bonds on membrane is typically nonhomogeneous [29]. In this section, we describe lubrication adhesive dynamics under four different adhesion scenarios, namely, no adhesion, uniform adhesion, clustered adhesion, and focal adhesion (Fig. 1).

1. No adhesion

For the case without adhesion ($\alpha=0$), a leading edge perturbation results in a traveling wave, whose amplitude decreases with time (Fig. 2, upper left). Since membrane tension is dominant, we generalize such waves as tension waves. The pressure wave assumes a "w-shape" profile with negative pressures at the wave front and rear (Fig. 2, lower left).

2. Uniform adhesion

For the case of uniform adhesion ($\alpha=2$, $\beta=4$, $X\geq 1$), the traveling wave shows an increase in amplitude (Fig. 2, upper right) and the pressure wave is dual peaked (Fig. 2, lower right). We generalize such waves as adhesion waves. The observed growth in wave amplitude is remarkable because the adhesive stress is tensile which tends to restore the gap height to the equilibrium length. Both the maximum gap height and pressure tend toward equilibrium at long times.

3. Clustered adhesion

For the case of clustered adhesion, the adhesion distribution is rendered nonuniform such that the adhesion bond density is saturated near the leading edge [33]. To illustrate the effects of adhesion distribution, we specify $\alpha=2$, $\beta=4$, $\bar{\chi}=4$, $\bar{\eta}=0.1$, $X\geq 1$. During entry into the cluster, the initial tension wave switches to an adhesion wave. However, as the adhesion wave progresses through the cluster, it reverts to a tension wave (Fig. 3, left).

4. Focal adhesion

Focal adhesion typically consists of a cluster of adhesive molecules of high mechanical stability. Focal adhesions are also known to fracture rather than peel [32]. In this study, we model focal adhesion as a strong uniform adhesion cluster, whose bonds do not rupture under stress ($\alpha=5$, $\beta=0$, $1\leq X\leq 5$). The bond distribution is given by $\phi(1\leq X\leq 5)=1$. As shown in (Fig. 3, right), the tension wave first collides into a stiff adhesion zone, trapping fluid and generating large pressures within the focal adhesion. Then it spreads rapidly along the length of the focal adhesion resulting in a highly dispersed wave. The pressure remains elevated for an extended period of time after the wave front has exited the focal adhesion.

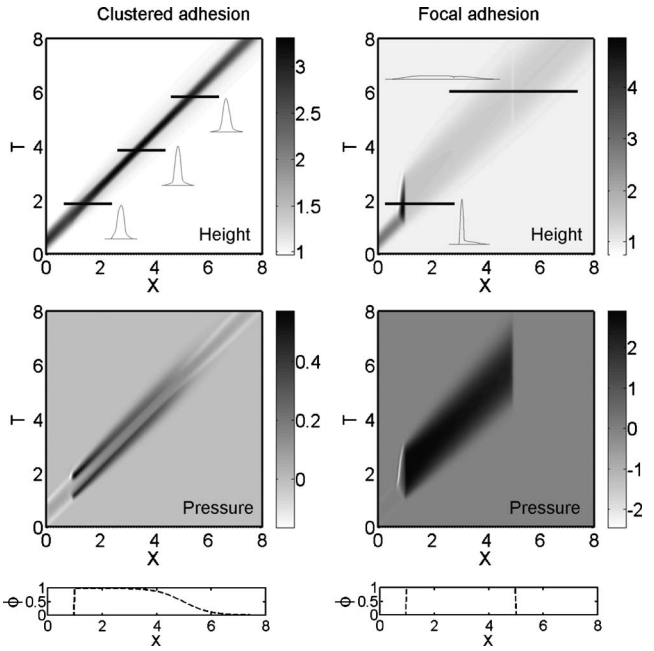

FIG. 3. Space-time plots of membrane height and pressure profile using perturbed amplitude $\epsilon=2$ and tension $\bar{\sigma}=1$. Bottom plots denote adhesive bond distribution $\phi(X)$. (Left) Clustering of adhesive bonds ($\alpha=2$, $\beta=4$, $\bar{\chi}=4$, $\bar{\eta}=0.1$, $X\geq 1$) results in the adhesion wave reverting to tension wave a distance from the leading edge; (right) focal adhesion ($\alpha=5$, $\beta=0$, $1\leq X\leq 5$) results in significant wave dispersion. Insets show wave profiles at specific times indicated by the adjacent cuts.

B. Wave transition

As observed in the preceding section, waves could manifest as either tension wave or adhesion wave. In this section, we analyze the physical conditions governing each type of wave and how wave transition could occur. First we define ΔH_m as the maximum wave amplitude within the adhesion zone ($X>1$) and ΔH^* as the reference maximum wave amplitude in the absence of adhesion ($\alpha=0$, $\bar{\sigma}=1$, $X>1$). We also define a wave with a reduced amplitude ratio ($\Delta H_m/\Delta H^*<1$) as a tension wave and one with an amplified amplitude ratio ($\Delta H_m/\Delta H^*>1$) as an adhesion wave. The wave transition point is defined at the crossover point ($\Delta H_m/\Delta H^*=1$).

1. Adhesive stress

Setting $\phi(X)=1$, the adhesive stress term in Eq. (8) is written as

$$M \equiv \alpha \Delta H \exp\left(-\frac{\beta \Delta H^2}{2}\right). \tag{10}$$

We plot adhesion stress M and its gradient $\partial_H M$ against membrane height H as shown in Fig. 4(a) for a range of adhesion probabilities $\beta=\{0,1/4,1,4\}$. At the edges of the wave, the membrane height tends toward the equilibrium value ($\Delta H\to 0$), where the adhesive stress ($M\to 0$) tends to zero and the adhesive gradient ($\partial_H M\sim\alpha$) is independent of height. Setting the adhesion gradient $\partial_H M$ to zero, we show that the maximum adhesion stress occurs at a critical gap height ($\beta^{-1/2}$). If the gap height is less than the critical value

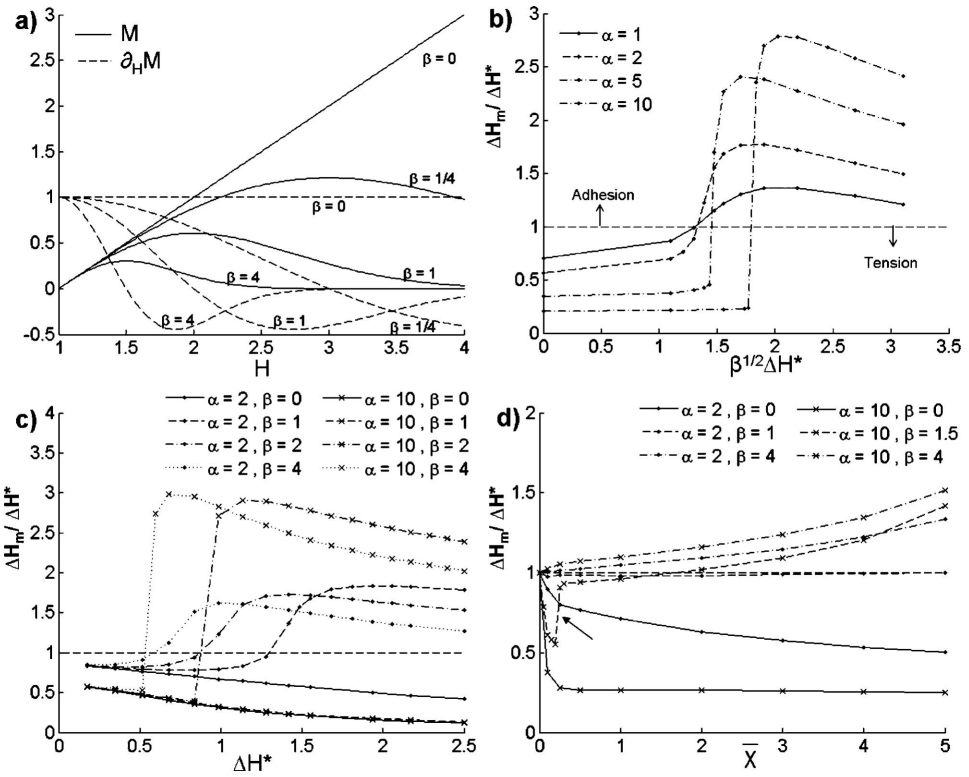

FIG. 4. (a) Plots of adhesive stress M and its gradient $\partial_H M$ against membrane height H; (b) plots of amplitude $\Delta H_m/\Delta H^*$ against transition parameter $\beta^{1/2}H^*$ ($\epsilon=2$, $\bar{\sigma}=1$); (c) plots of amplitude $\Delta H_m/\Delta H^*$ against reference amplitude ΔH^* ($\bar{\sigma}=1$); (d) plots of amplitude $\Delta H_m/\Delta H^*$ against adhesive cluster size $\bar{\chi}$ ($\bar{\sigma}=1$).

($\Delta H < \beta^{-1/2}$), adhesion is dominated by the bond stiffness, leading to tension waves. Conversely, if the gap height is greater than the critical value ($\Delta H > \beta^{-1/2}$), adhesion is dominated by binding kinetics, leading to adhesion waves. This argument suggests that a criterion for tension to adhesion wave transition is $\beta^{1/2}\Delta H^* > 1$.

2. Wave transition criterion

We plot the maximum wave amplitude $\Delta H_m/\Delta H^*$ against the transition parameter ($\beta^{1/2}\Delta H^*$) as shown in Fig. 4(b), where $\epsilon=2$ and $\alpha=\{1,2,5,10\}$. We observe that the transition points are consistently greater than unity, which agrees with the criterion for wave transition ($\beta^{1/2}\Delta H^* > 1$). In addition, we found that an increase in adhesion strength α leads to dispersion in tension waves but amplification in adhesion waves. This disparity results in sharp tension to adhesion wave transition points under strong adhesion.

3. Criterion is insufficient

We plot the maximum amplitude $\Delta H_m/\Delta H^*$ against the reference wave amplitude ΔH^* as shown in Fig. 4(c), using a range of adhesion strengths $\alpha=\{2,10\}$ and adhesion probabilities $\beta=\{0,1,2,4\}$. If $\beta=0$, no adhesion wave transition is observed at any adhesion strength α, following the transition criterion. If $\beta=0$, wave transition is readily observed under weak adhesion ($\alpha=2$), but not under strong adhesion ($\alpha=10$), even under exceedingly large reference wave amplitudes ΔH^*. The tension wave is sufficiently stable that wave transition does not even occur. This shows that $\beta^{1/2}\Delta H^* > 1$ is a necessary but insufficient criterion for wave transition.

4. Transition depends on adhesion size

Finally we examine the case of nonuniform adhesion. We plot the maximum amplitude $\Delta H_m/\Delta H^*$ against the adhesion cluster length $\bar{\chi}$ ($\bar{\sigma}=1$) as shown in Fig. 4(d). For the case of weak adhesion ($\alpha=2$), the amplitude of a tension wave ($\beta=0$) decreases nonlinearly with $\bar{\chi}$, whereas the amplitude of an adhesion wave ($\beta=4$) increases linearly with $\bar{\chi}$. If ($\beta=1$), the contributions due to adhesion and tension cancel out sufficiently that $\Delta H_m/\Delta H^*$ is nearly independent of $\bar{\chi}$. We note that there is no observable wave transition at low adhesion strengths.

For the case of strong adhesion ($\alpha=10$), the amplitude of a tension wave ($\beta=0$) decreases rapidly with $\bar{\chi}$ until an equilibrium is reached at approximately 0.25, whereas the amplitude of an adhesion wave ($\beta=4$) increases linearly with $\bar{\chi}$. Remarkably, for ($\beta=3/2$), we observe a sharp jump in amplitude at $\bar{\chi}\sim 0.3$, followed by a transition from tension to adhesion wave. This result shows wave transition could occur under strong adhesion and it depends on the relative size of the adhesion cluster. In contrast, we note that the wave amplitude $\Delta H_m/\Delta H^*$ is relatively insensitive to the exponential prefactor $\bar{\eta}$, which describes the shape of the adhesion distribution function (results not shown).

IV. CONCLUSION

We review briefly the main findings of the present paper. Membrane waves are found to exist as either tension or adhesion waves depending on competitive tension and adhesion effects. In contrast to tension waves, adhesion waves show characteristically amplified peaks and are highly persistent. The transition of tension to adhesion waves is found to depend on a necessary but insufficient criterion ($\beta^{1/2}\Delta H^* > 1$). Strong adhesion results in sharp tension-to-adhesion wave transitions.

The biological relevance of lubrication adhesive dynamics deserves mention. Owing to limited experimental data, it is difficult to conclude whether the protrusion traveling waves observed on adhered cell membranes are tension or adhesion waves. Images obtained from differential inference contrast (DIC) microscopy and plotted on kymographs show highly persistent waves, whose wavelengths first increase and later decrease with time, shortly after leading edge retraction [1]. These observations support the presence of adhesion waves as opposed to tension waves, which tend to disperse. On a different note, it would be interesting if DIC kymographs can be superimposed on vinculin-stained images with reference to the positions of focal contacts and adhesions [3]. This can elucidate membrane behavior, such as the extent of wave dispersion, in the presence of localized adhesion structures, such as focal adhesions.

Owing to protrusion forces, it is possible for the lamellum to separate from the membrane. Fluid is trapped between the lamellum and the membrane, instead of between the membrane and the substrate [1]. Since the lamellum and membrane layers are held by adhesive molecules, the present lubrication adhesive dynamics model remains applicable. However, since the adhesion force required for lamellum separation ($\sim$150 pN/μm) [37] is closely matched by protrusion forces [38–40], its occurrence is by no means definitive. Similar membrane delamination is involved in a related problem of blebbing, where an asymmetry in retraction could result in traveling bleb phenomenon (see Appendix B).

Our findings could be extended to two dimensional cell membranes even though we do not expect any significant difference compared to the current results. Nevertheless, we noted that focal adhesions have limited sizes so that membrane waves far away are expected to encounter less resistance. This aspect could be further investigated.

The present lubrication adhesive dynamics model is minimal. First, the fixed point perturbation model adopts a simplistic view of the protrusion event, whose physics is complex and largely unknown currently. Second, the model does not account for slow kinetics, where the time scale of bond formation and breakage is significant, as well as catch-slip bond behavior, where bond strengthen on extension [41]. Lastly, we assume that there are no significant biochemical processes affecting the wave dynamics. Despite such limitations, the present model explains the coupled physics behind lubricated adhesive membranes and it represents a first step toward the elucidation of biological problems involving membrane adhesion and thin liquid films.

ACKNOWLEDGMENT

The authors wish to thank J. K. White and L. Mahadevan for their invaluable comments and suggestions.

APPENDIX A: BOUNDARY LAYERS

Inspection of Eq. (8) shows that if the bending term is neglected ($\bar{\gamma}\to 0$), the order of equation is reduced by two so that two out of the original six boundary conditions cannot be satisfied. This implies that even in a tension-dominated regime ($\bar{\sigma}\gg\bar{\gamma}$), a boundary layer exists within which bending effects cannot be neglected. Balance of the bending and tension terms yields an estimate of the bending boundary layer thickness $(\xi/L)\sim(\gamma/\sigma L^2)^{1/2}$.

If, in addition, the tension term is neglected ($\bar{\sigma}\to 0$), the order of equation is further reduced by two. Thus, even in the adhesion-dominated regime ($\alpha\gg\bar{\sigma}$), a tension boundary layer exists whose thickness is $(\delta/L)\sim(\sigma/A_t K_{eq}\kappa L^2)^{1/2}$.

If $0<\xi<\delta$, the respective boundary layers are nested, such that the bending boundary layer is confined within the tension boundary layer. Membrane behavior is governed by different regimes under different length scales.

APPENDIX B: TRAVELING BLEBS

Blebs are blisterlike protrusions of the cell surface that appear and disappear from the surface of a cell [42]. The formation of blebs is thought to be initiated by the separation of the cell membrane from the cortex [43]. Some long-lived blebs, commonly observed in embryonic blastomeres, are observed to travel tangentially along the cell surface in a persistent manner [44]. One question we ask is whether there is a simple physical explanation for such traveling phenomenon.

Consider a flexible cell membrane adhered to an immovable cortex, which is assumed to be impenetrable to fluid. The dimensional lubrication adhesive dynamics equations are

$$\partial_t h-\frac{1}{12\mu}\partial_x(h^3\partial_x p)=0, \tag{B1a}$$

$$(p-p_c)-A_b\kappa(h-\lambda)+\sigma\partial_{xx}h-\gamma\partial_{xxxx}h=0. \tag{B1b}$$

Using a small perturbation on the gap height $h=\lambda+h'$, where the disturbance is expressed in the form $h'=h_0'\exp(ikx+st)$, we linearize the equations around the equilibrium gap height $h=\lambda$ and obtain a characteristic equation for the growth rate s,

$$\left(\frac{12\mu}{\lambda^3}\right)s=2ik\partial_x(A_b\kappa)+\partial_{xx}(A_b\kappa)-(A_b\kappa k^2+\sigma k^4+\gamma k^6), \tag{B2}$$

where the first term on the right-hand side is imaginary and produces traveling wave solutions with phase speed $\mathrm{Im}(s/k)=(\lambda^3/6\mu)\partial_x(A_b\kappa)$. Hence, it is clear that any nontrivial spatial adhesion gradient is sufficient to produce tangential motion in a perturbation. There is no additional requirement for external forcing. Although the actual size of a bleb is larger than what can be considered as a minor perturbation, sustained traveling motion in blebs can be expected to be driven through local gradients of adhesion or an asymmetric retraction of actomyosin cortex [44].

As a side note, if the adhesion curvature term is greater than the sum of all the dissipative terms, i.e., $\partial_{xx}(A_b\kappa)>(A_b\kappa k^2+\sigma k^4+\gamma k^6)$, then the real part of the growth rate $\mathrm{Re}(s)>0$ and instability occurs. This suggests that it is physically possible for bleb growth to occur, even transiently, during a bleb retraction phase.

[1] G. Giannone, B. J. Dubin-Thaler, O. Rossier, Y. Cai, O. Chaga, G. Jiang, W. Beaver, H. Döbereiner, Y. Freund, G. Borisy, and M. P. Sheetz, Cell **128**, 561 (2007).
[2] G. Giannone, B. J. Dubin-Thaler, H. Döbereiner, N. Kieffer, A. R. Bresnick, and M. P. Sheetz, Cell **116**, 431 (2004).
[3] L. Ji, J. Lim, and G. Danuser, Nat. Cell Biol. **10**, 1393 (2008).
[4] W. Helfrich, Z. Naturforsch. C **28**, 693 (1973).
[5] S. A. Safran, *Statistical Thermodynamics of Surfaces, Interfaces, and Membranes* (Addison-Wesley, New York, 1994).
[6] F. Brochard and J. F. Lennon, J. Phys. (France) **36**, 1035 (1975).
[7] U. Seifert, Phys. Rev. E **49**, 3124 (1994).
[8] N. Gov and A. Gopinathan, Biophys. J. **90**, 454 (2006).
[9] Lawrence C.-L. Lin and F. L. H. Brown, Phys. Rev. Lett. **93**, 256001 (2004).
[10] Lawrence C.-L. Lin and F. L. H. Brown, Phys. Rev. E **72**, 011910 (2005).
[11] J. Prost, J. B. Manneville, and R. Bruinsma, Eur. Phys. J. B **1**, 465 (1998).
[12] J. Prost, J. B. Manneville, and R. Bruinsma, Europhys. Lett. **33**, 321 (1996).
[13] J. B. Manneville, P. Bassereau, D. Lévy, and J. Prost, Phys. Rev. Lett. **82**, 4356 (1999).
[14] S. Ramaswamy, J. Toner, and J. Prost, Phys. Rev. Lett. **84**, 3494 (2000).
[15] N. Gov, A. G. Zilman, and S. Safran, Phys. Rev. E **70**, 011104 (2004).
[16] R. Shlomovitz and N. S. Gov, Phys. Rev. Lett. **98**, 168103 (2007).
[17] J. T. Groves, Annu. Rev. Phys. Chem. **58**, 697 (2007).
[18] A. Oron, S. H. Davis, and S. G. Bankhoff, Rev. Mod. Phys. **69**, 931 (1997).
[19] S. R. Hodges and O. E. Jensen, J. Fluid Mech. **460**, 381 (2002).
[20] S. Reboux, G. Richardson, and O. E. Jensen, Proc. R. Soc. London, Ser. A **464**, 447 (2008).
[21] G. I. Bell, Science **200**, 618 (1978).
[22] M. Dembo, D. C. Torney, K. Saxman, and D. A. Hammer, Proc. R. Soc. London, Ser. B **234**, 55 (1988).
[23] D. Gallez and W. T. Coakley, Prog. Biophys. Mol. Biol. **48**, 155 (1986).
[24] D. Gallez, A. De Wit, and M. Kaufman, J. Colloid Interface Sci. **180**, 524 (1996).
[25] A. E. Hosoi and L. Mahadevan, Phys. Rev. Lett. **93**, 137802 (2004).
[26] E. A. Evans, Biophys. J. **48**, 175 (1985).
[27] P. A. DiMilla, K. Barbee, and D. A. Lauffenburger, Biophys. J. **60**, 15 (1991).

[28] D. A. Hammer and D. A. Lauffenburger, Biophys. J. **52**, 475 (1987).
[29] E. Zamir and B. Geiger, J. Cell. Sci. **114**, 3583 (2001).
[30] C. Le Clainche and M. F. Carlier, Physiol. Rev. **88**, 489 (2008).
[31] E. A. Wayner, R. A. Orlando, and D. A. Chresh, J. Cell Biol. **113**, 919 (1991).
[32] M. D. Ward and D. A. Hammer, Biophys. J. **64**, 936 (1993).
[33] N. D. Gallant and A. J. García, J. Biomech. **40**, 1301 (2007).
[34] D. Kong, B. Ji, and L. Dai, J. Theor. Biol. **250**, 75 (2008).
[35] T. W. Secomb, Biophys. J. **54**, 743 (1988).
[36] F. Chamaraux, O. Ali, S. Keller, F. Bruckert, and B. Fourcade, Phys. Biol. **5**, 036009 (2008).
[37] M. P. Sheetz, Nat. Rev. Mol. Cell Biol. **2**, 392 (2001).
[38] V. C. Abraham, V. Krishnamurthi, D. L. Taylor, and F. Lanni, Biophys. J. **77**, 1721 (1999).
[39] S. Bohnet, R. Ananthakrishnan, A. Mogliner, J. J. Meister, and A. B. Verkhovsky, Biophys. J. **90**, 1810 (2006).
[40] S. Felder and E. L. Elson, J. Cell Biol. **111**, 2513 (1990).
[41] Y. J. Wei, Phys. Rev. E **77**, 031910 (2008).
[42] G. T. Charras, J. Microsc. **231**, 466 (2008).
[43] G. T. Charras, J. C. Yarrow, M. A. Horton, L. Mahadevan, and T. J. Mitchison, Nature (London) **435**, 365 (2005).
[44] G. T. Charras, M. Coughlin, T. J. Mitchison, and L. Mahadevan, Biophys. J. **94**, 1836 (2008).